2-1-2017

Metastable States in Terminal Orientation of Hinged Symmetric Bodies in a Flow

Doralia Castillo
Montclair State University

Bong Jae Chung
Montclair State University, chungb@mail.montclair.edu

Klaus Schnitzer
Montclair State University, schnitzerk@mail.montclair.edu

Karina Soriano
Montclair State University

Haiyan Su
Montclair State University, suh@montclair.edu

See next page for additional authors

International Journal of Engineering Science 111 (2017) 19–27

Contents lists available at ScienceDirect

International Journal of Engineering Science

journal homepage: www.elsevier.com/locate/ijengsci

Metastable states in terminal orientation of hinged symmetric bodies in a flow

D. Castillo[a], B. Chung[c], K. Schnitzer[b], K. Soriano[a], H. Su[a], A. Vaidya[a,*]

[a] Complex Fluids Laboratory, Department of Mathematical Sciences, Montclair State University, Montclair, NJ 07043, United States
[b] Department of Art and Design, Montclair State University, Montclair, NJ 07043, United States
[c] Department of Bioengineering, George Mason University, Fairfax, VA 22030, United States

ARTICLE INFO

Article history:
Received 21 April 2016
Accepted 9 November 2016
Available online 21 November 2016

Keywords:
Fluid-solid interaction
Metastability
Terminal orientation
Steady state

ABSTRACT

Symmetric bodies such as cylinders and spheroidal bodies, in their terminal stable states, are long known to have their long axis align themselves perpendicular to the direction of the flow. This property has been confirmed in primarily sedimentation based theoretical, experimental and numerical techniques and the transition to a terminal stable state is believed to coincide with the onset of significant inertial effects in the flow. However, the threshold at which this transition occurs is yet unknown. We conduct modified experiments with hinged bodies and a CFD study to examine the nature of the transition of prolate spheroids and cylinders of various aspect ratios, from initial to their terminal stable equilibrium. Our experiments and numerics, both reveal the presence of intermediate *metastable states* which are sensitive to the flow Reynolds number and physical attributes of the immersed body and gradually lead to the stable state.

1. Introduction

The terminal state of a freely sedimenting body in a fluid includes its terminal velocity as well as the terminal orientation. While the former is often discussed, even in elementary physics courses, the latter is less well known. The scientific community is aware for some time now that rigid bodies, when dropped in a quiescent liquid, will orient themselves in certain ways with respect to the direction of gravity (Kirchoff, 1869; Lamb, 1895). The orientation is seen to depend upon the shape of the body and also upon the nature of the fluid in which it is immersed. However, in a highly viscous fluid, in the creeping flow regimes, the body is seen to maintain its initial orientation with time (Leal, 1980). As inertial forces begin to dominate, the rotational axis (a) of the falling body is eventually seen to become perpendicular to the direction of gravity. A sedimenting cylinder, for instance, is known to fall with its axis of symmetry (a) perpendicular to gravity in a Newtonian fluid provided its length, l, exceeds its diameter, d. When $l < d$, the body falls with its axis a parallel to the direction of gravity. There is extensive work on the terminal states of cylinders and spheroids in a variety of fluid environments, Newtonian and non-Newtonian (Blevins, 1977; Galdi, 2002; Joseph & Liu, 1993; Lamb, 1895; Vaidya, 2006; Zdravkovich, 1997; 2002). There are also several studies devoted to the sedimentation of *thin* bodies such as filaments, disks or falling paper (Belmonte, Eisenberg, & Moses, 1998; Fields, Klaus, Moore, & Nori, 1997; Kirchoff, 1869; Mahadevan, Ryu, & Samuel, 1999; Tanabe & Kaneko, 1994). The most comprehensive experimental study on the terminal orientation of sedimenting *isometric*

* Corresponding Author. Fax: 973 655 7686.
E-mail address: vaidyaa@mail.montclair.edu (A. Vaidya).

http://dx.doi.org/10.1016/j.ijengsci.2016.11.004
0020-7225/

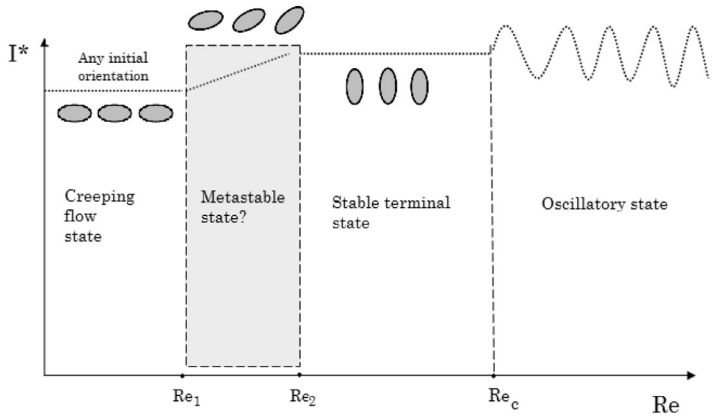

Fig. 1. A schematic of the phases that an immersed body undergoes in a fluid. The existence and details of a transition from the creeping flow regime to terminal stable state is not yet known and is the subject of this paper. We argue in favor of a continuous transition (shaded region) rather than a discontinuous jump. In other words, we show that $Re_2 - Re_1 > 0$ is more likely than $Re_2 - Re_1 = 0$.

bodies dates back to 1948, due to Pettyjohn and Christiansen (Pettyjohn & Christiansen, 1948) who examined the falling behavior of a wide class of polygonal bodies.

While the majority of previous papers have been pursued via sedimentation, there is a drawback with this method; these studies are restricted by the short fall times and do not allow for complete control over the terminal fall speed, and hence the Reynolds number. The same steady state, seen during sedimentation, can also be observed in experiments where the particle is hinged at the center of a flow tank (see Fig. 2) while allowing the fluid to move past it Camassa, Chung, Howard, McLaughlin, and Vaidya (2010). In such horizontal flow constructions(in water and wind tunnels), there has been a lot of attention paid to the unsteady dynamics of bodies and the unsteady response of disks in aerodynamic flows (Chung, Cohrs, Ernst, Galdi, & Vaidya, 2016; Lugt, 1980; 1983; Williamson, 1996; Williamson & Goverdhan, 2004; Willmarth, Hawk, Galloway, & Roos, 1967). The current paper is devoted to the orientational reconfiguration of symmetric bodies (cylinders and spheroids) just beyond the creeping flow regimes and before the onset of unsteady flow characteristics. Experiments where the translational motion is suppressed but the rotational forces are preserved, could be preferable for such studies since they allow for longer observation times without changing the physics of the problem.

Experiments under both types of setups (Camassa et al., 2010; Chung et al., 2016; Fields et al., 1997) have revealed that terminal states are subject to the constraint of flow speeds, particle density and length and can be well characterized by the dimensionless numbers Re(Reynolds number) and I^* (dimensionless inertia) which reveal various phases and bifurcations.[1] For sufficiently small Re, the body achieves the steady equilibrium discussed earlier. However, as Re exceeds a critical threshold, the body moves to display various time-dependent periodic motions (Camassa et al., 2010; Lugt, 1980; Willmarth et al., 1967). The focus of this study remains in the earlier, yet, unexplored aspect of the problem at low Re.

Theoretically, in the case of sedimentation, one could explain the stable orientation configurations of the body as based on the vanishing of the net torque imposed on it by the fluid due to viscous and inertial effects (Galdi & Vaidya, 2001). The net torque imposed by the surrounding fluid at $O(Re)$ is given by the expression

$$\vec{\mathcal{M}} = Re\,\alpha\,\sin 2\theta\,\hat{e}_3 \tag{1}$$

where α is the torque coefficient which depend upon the geometry and physical properties of the rigid body. The zeros of Eq. (1) reveal the two equilibrium orientation, namely 0° and 90°, of the sedimenting body, but does not contain any information about any intermediate or metastable states. Overall, theoretical arguments rely on the underlying hypothesis that a body, in a fluid, turns to its terminal orientation along with the development of a steady symmetric wake vortex. Bifurcation to an unsteady, asymmetric vortex then leads to the subsequent oscillatory (including flutter and tumbling) phases of the body (Chung et al., 2016).

Despite of the wealth of information available on this subject, some significant questions remain unanswered: (**Q1**) What is the Re at which a cylindrical body, say, transitions from its initial orientation to the final perpendicular state? (**Q2**) Is this transition a smooth one or a sudden jump across a critical Re? Q2 also begs the question if there are intermediate metastable states that the cylinder assumes (see Fig. 1)? This paper is devoted to the resolution of these questions by means of a horizontal flow, hinged body experiment and computational fluid dynamics (CFD) approach to study the orientation of symmetric bodies as a function of flow speed, particle geometry and density.

[1] In our study, we use cylinders and spheroids for which our non-dimensional parameters are defined as follows: $Re = \frac{\rho U d}{\mu}$ where U is the characteristic velocity, ρ is the fluid density, d is the length of the longest axis of the body facing the flow and μ is the fluid viscosity. Also $I^* = \frac{I}{\rho_b l^4 a}$ where I is the moment of inertia of the body, l is the length of the axis of rotation and a is the diameter.

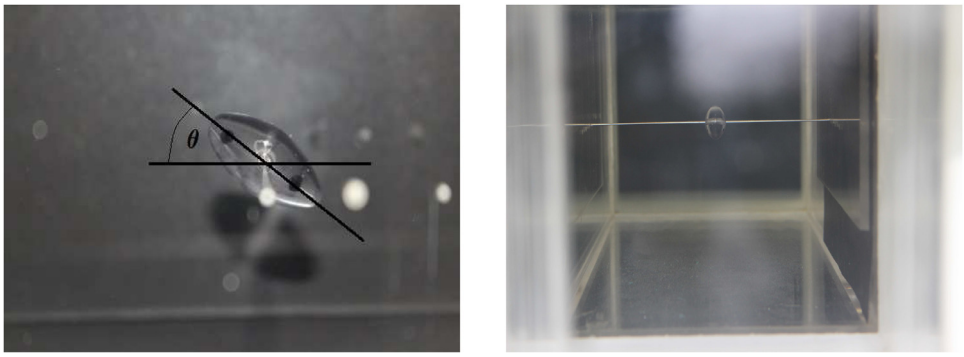

Fig. 2. Figures (a) and (b) depict the experimental setup from different perspectives. The spheroidal and cylindrical bodies used in this study are hinged at their center allowing for one degree of rotational freedom. Flow in image (a) goes from left to right and out of the page in panel (b). The panel (a) also depicts how the orientation angle, θ, is measured.

Table 1
Dimensions and material parameters for the bodies used in the study.

	Shape	Name	Material	Density(gms/cc)	Aspect ratio($\frac{L}{D}$)	I^*
1.	Spheroid	S1,SW1	Wax	0.9	2.0	0.021
2.	Spheroid	S2	Plexiglass	1.18	2.0	0.028
3.	Cylinder	C2.0	Plastic(Abs)	1.04	2.0	0.040
4.	Cylinder	C1.25,CW1.25	Plastic(Abs)	1.04	1.25	0.081
5.	Cylinder	C1.0	Plastic(Abs)	1.04	1.0	0.119
6.	Cylinder	C0.75	Plastic(Abs)	1.04	0.75	0.212

2. Experiments

2.1. Methods

Our experimental setup consisted of prolate spheroids and cylinders hinged at the center of a water tunnel (Engineering Laboratory Design Inc., Model 502) capable of flow rates between 0.1–1.0 fps at 0.5 hp(see Fig. 2). The dimensions of the test section of the water tunnel are $6 \times 6 \times 18$ in.. The cylinder was held in place by means of a stainless steel rod of thickness 1–2.5 mm passing through the rigid bodies, which were placed in such a way as to prevent any translational motion. The bodies were fitted with miniature ball bearings with inner diameter of 1 mm through which the rods were secured.

We examined eight experimental cases (Table 1) with different bodies. These consisted of two prolate spheroidal bodies of diameter 0.5 in. and eccentricity 0.86, one made of plexiglass and the other of wax. Additionally four plastic cylinders (ABS) of dimater 0.5 in. and varying aspect ratios (2,1.25,1 and 0.75) were also used. The horizontal setup naturally raises questions about the effects of friction in our observations. To address the impact of friction, two different experimental setups were considered; in addition to using rods and ball bearings, we also used a setup where the bodies were suspended by means of a taut copper wire (thickness 0.023 cm) placed through the center of the bodies, in the absence of ball bearings (indicated by SW1 and CW1.25). Such a setup was also employed in a previous study by Camassa et al. (2010). The particles were exposed to flow speeds ranging from 0 to 13.6 cm/s while maintaining each speed up to several minutes, in order to allow the particle to reach a steady orientation and the flow perturbations to die out. Images of the particle in its steady orientation and wake structure were recorded using a Nikkon D800 camera with a 105 mm f2.8 macro lens with exposure f5.6–f8. In order to visualize the wake structure, the flow was seeded with microscopic hollow glass spheres of average diameter 13 μm and illuminated using a laser sheet (532 nm, 1 W laser from Opto Engine LLC). The images were taken under a low ISO setting and for exposure times between 0.5 and 2/3 s with the camera placed orthogonal to the flow (see Fig. 3(b)). The angle of orientation of the body is defined as the angle between the $-x$ axis and axis of symmetry of the body (see Fig. 2). The Reynolds numbers in the experiments ranged between 100–5000.

In order to address the questions (**Q1**) and (**Q2**) outlined in the introduction (Fig. 1), the experimental procedure involved photographing the various bodies at different *Re* until the onset of the terminal stable steady orientation (i.e. until the symmetry axis of the body became perpendicular to the flow direction). The *Re* in each individual case was modified by changing the flow speed (whose increments were restricted by the limits of the pump characteristics). For sake of repeatability, we attempted to vary the initial angle of suspension of the body but in some cases were forced on rely on the angle assumed by the body which was shifted from the desired angle by small perturbations to the system. A total of 49 trials, for all bodies, were conducted with several flow speeds considered in each trial.

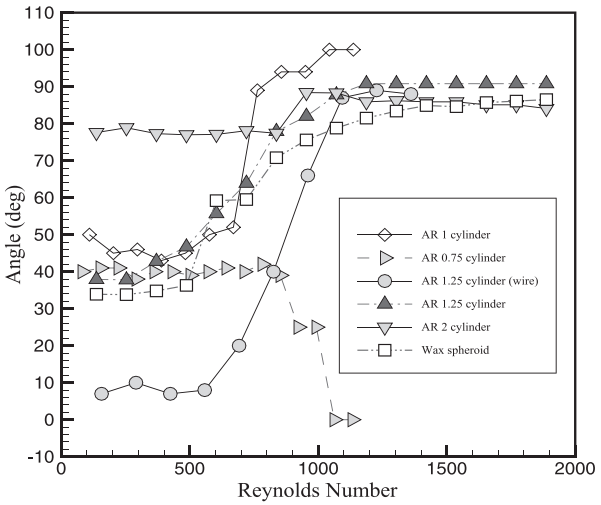

(a)

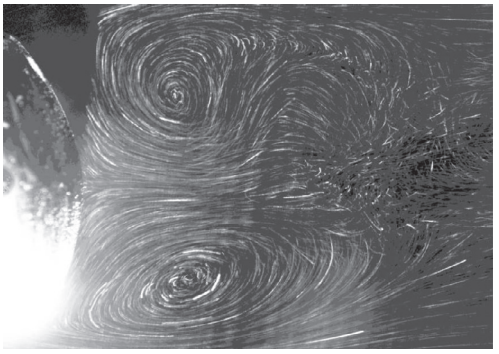

(b)

Fig. 3. The panel (a) depicts the variation in orientation angle as a function of *Re*. Any deviation from 90° in the terminal orientation results from possible measurement, machining and manufacturing errors (i.e. slight asymmetry of the spheroids and cylinders). Panel (b) shows a representative flow visualization image of the wake vortex at $Re \approx 700$. The flow was seeded with microscopic hollow glass spheres and illuminated using a laser sheet orthogonal to the viewing angle and along the central plane of the body.

We use statistical analysis to answer the questions raised earlier. Specifically, statistical investigation can help reveal repeatable patterns and correlations between orientation angle and flow speed. The scatter plot of the observed orientation angle and *Re* shows nonlinear pattern of the relationships, which suggests that nonparametric models should be fitted to study those relationships. Among the nonparametric models, generalized additive model (Hastie & Tibshirani, 1990) was used to fit the data in this study because it allows the continuous predictors to be fitted by using a smoothing method while keeping other categorical predictors in the model. Local nonparametric regression models (Ruppert, Sheather, & Wand, 1995), which estimate the smooth function of the predictor by fitting a polynomial model within a sliding window, was fitted and plotted with the original observed data to display the relationship between the orientation angle and flow. All the statistical analysis was conducted by using the statistical software R 3.1.1.(Team, 2013) and results are tabulated in appendix A.

2.2. Results

The main observations of our experiments are summarized in the Fig. 3 which show the steady orientation for varying *Re*. While the details of the patterns that emerge are slightly different depending upon the particle geometry, aspect ratio and initial orientation, some commonalities are observed: (i) For all particles, the transition from the initial state to the terminal stable equilibrium[2] of 90° is gradual and proceeds through intermediate angles (possible metastable states). In cases when the particle is already near another equilibrium (namely $\theta = 0$ deg), the initial state can persist and the change to the more stable state can be a more drastic jump. But even in such cases the spheroid/cylinder is seen to reconfigure itself in a somewhat continuous manner. We hypothesize the presence of a critical *Re*, denoted Re_1, depending on particle features and initial angle, beyond which the transition is seen to occur and a second critical value, Re_2, beyond which the terminal state is achieved (Fig. 1).

Rigorous non-parametric statistical analysis was performed to check for the significance of the effects of Reynolds number upon the orientation angle. Three sets of generalized additive models (Hastie & Tibshirani, 1990) were performed in three stages corresponding to three different groupings of the data. In the first model, each trial corresponding to a material type and phase was fitted into one model. For the 49 combined trials considered in this study, we modeled the relationship between the orientation angle and Reynolds number using additive models where the non-parametric function of Reynolds number was estimated using a smoothing method. Except for certain trials where additive model could not fit the data due to the lack of unique observations, for most of the 49 trials, we found the additive models fit the data very well with a highly significant *p* value, which indicated that there is indeed a nonlinear relationship between the orientation angle and Reynolds number. The model fit statistic adjusted R^2 range and deviance explained value range are reported in Table 2 for the same type of material. Two fitted models using local nonparametric fitting methods (Ruppert et al., 1995) with original data are also plotted to show the nonlinear relationship between Reynolds number and the angle.

[2] The single case of $AR < 1$, indicated by the symbol ▷ eventually settles to the terminal stable orientation state of 0° which is consistent with previous observations (Chung et al., 2016).

For the second set of models, the tests were separated by the particle type (S1,S2 etc.) and dimensions. All different trials of any single particle were grouped together in this analysis. For each material type (8 in total) with all trials combined, two different models were fitted separately based on the phases. Because there were big variability in initial angles among different trials, not all non-parametric models fit the data well, but for material S1 in the phase 1 and S2 in the phase 2, it showed strong nonlinear relationships between the angle and the Reynolds number. It must be kept in mind that for a given particle type, the different trials often had different initial angles which contributed to the poor collective fits. Adjusted R^2, deviance explained value and p-value were also reported for these models in Table 2.

Lastly, with all 49 trials together, we fit a generalized additive model to discern the nonlinear relationship between angle with Reynolds number by controlling the material type and phase. The fitted model is reported in Table 3. This model indicates that the phase, the material type and the Reynolds number all significantly affect the angle. Specifically, the Reynolds number has a significant nonlinear relationship with the angle (empirical distribution function, edf $= 3.725$, p-value $= 0$).

While the above observations and statistical analysis seem to confirm the presence of intermediate equilibria for all the bodies used in the experiments, these states can also be induced by friction which try as one may, cannot be eliminated in experiments.[3] It must be emphasized that the presence of friction does not invalidate our experimental claims which are reflective of the physics experienced in real world scenario. In the presence of friction, the hinged bodies experience a critical resistance force when a torque acts on it (assume the torque to be of the form given by Eq. (1)). If the torque exceeds this critical, frictional force, then the body is likely to turn to its next equilibrium point which occurs at the angle where torque balances the frictional force. When the initial torque is low, the body stays in its initial position. Such a constant frictional resistance force can cause the body to slowly transition from its initial position to the most stable state (usually 90°) showing the profile seen in Fig. 3. These transitional states continue to exist in our experiments for bodies of different shapes and masses which suggests variation in magnitude of friction. However, even if the observations were induced by friction, the question remains if metastability would persist when frictional forces vanished. This question must necessarily be verified by computation which is discussed below.

3. CFD analysis

In this section we discuss the results of numerics performed for independent verification of the existence of metastable states. While our experiments hints at the possibility of metastability in a real world scenario, CFD calculations can yield an added layer of validation and can reveal their presence in an absolute sense, i.e. in the absence of friction. We solve for the flow past a stationary spheroid for specific cases of Re and compute the resulting torque. Specifically, we are seeking torque free angles of the body as function of Re and AR.

3.1. Methods

We employ the immersed boundary (IB) method to study the problem numerically. This method is used to solve both, fluid flow and also the motion of bodies embedded in the fluid domains, (see Mittal and Iaccarino, 2005 for details). Numerically, the immersed bodies treated in our study (prolate spheroids with Aspect Ratio = 1.3, 2.0, 4.0, and 8.0) are generated and meshed using Freecad (Falck & Collette, 2012) and Gmsh (Geuzaine & Remacle, 2009) softwares, respectively. The fluid is considered to be linearly viscous and incompressible. The three dimensional Navier-Stokes equation is discretized by the finite difference method, and the series of discretized equations are solved explicitly by Adams Bashforth time steps. The fluid domain is represented by a rectangular box. A uniform flow profile, (U, 0, 0), is imposed at the inlet east boundary, while convective boundary condition is applied at the west outlet, which uses the constant inlet flow speed, U such that

$$\frac{\partial \vec{u}}{\partial t} + U\frac{\partial \vec{u}}{\partial x} = 0. \tag{2}$$

Here, $\vec{u}$ and x are the velocity and the flow direction, respectively (Sohankar, Norberg, & Davidson, 1998). Perfect slip boundary conditions are applied at the boundaries of computational domain elsewhere. We do not consider hydrostatic pressure in the z direction, hence gravitational force is ignored in the momentum equations.

The torque on the body, $\vec{\mathcal{M}} = (\mathcal{M}_1, \mathcal{M}_2, \mathcal{M}_3)$, can be computed by integrating the cross product of the force at a point of particle surface due to the flow and the corresponding radius vector (r_i) from the particle origin, given by

$$\mathcal{M}_i = \int \epsilon_{ijk}\, r_j\, p\, n_k\, dS + \int \epsilon_{ijk}\, r_j\, \tau_{km}\, n_m\, dS \tag{3}$$

where $i = 1, 2, 3$, S is the surface of the body and n is the outward unit normal.

The meshes in the fluid domain were refined in the region of the particle in vertical direction creating a total of around 7 million finite cubic fluid elements. The code was validated through the study of flow past a sphere at $Re = 500$, where we find the computed drag coefficient to be in good agreement with the data in the literature (Clift, Grace, & Weber, 2005). Other calculations on ellipses also yield results which are in agreement with know results, which lends additional support

[3] See also similar comments by Horowitz, M., and Williamson (2010) on a different FSI problem.

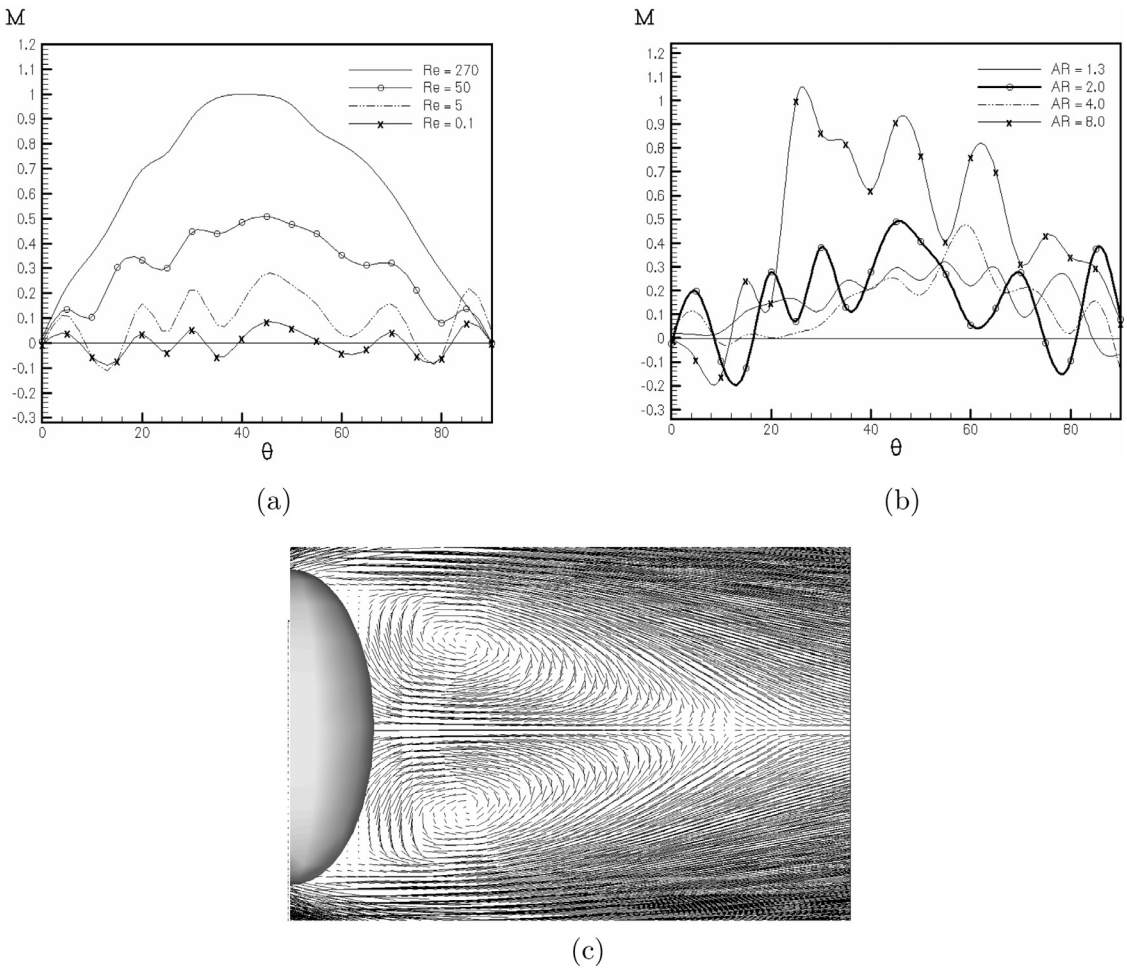

Fig. 4. Panel (a) shows the normalized magnitude of torque, $\mathcal{M}_3$ on an ellipsoid versus orientation angle, θ, subjected to a uniform flow at $Re = 0.1, 5, 50$ and 270. Panel (b) shows the impact of aspect ratio (AR) upon the torque profile. Panel (c) shows a representative flow field past a spheroid at $Re = 270$.

to our computations. These will be discussed below. Our calculations of flow past an ellipse, with the aspect ratio 2.0 were performed to identify a critical Reynolds number, Re_c, where the symmetric flow pattern is seen to transition to unsteady mode and is seen to occur at $Re_c \approx 360$. Consequently, to explore metastability, we considered the range of Re in which the flow is steady. We simulated the flow past a stationary ellipsoid oriented at different angles of attack ($0° < \theta < 90°$). These computations were performed at $Re = 0.1, 5, 50$ and 270. Fig. 4(c) shows a representative flow field in the wake region of the spheroid for the case of $Re = 270$.

3.2. Results

The computational simulation of the flow past an ellipsoid also prove that there are metastable configurations of a body in a flow for angles other than 0° or 90°. The central result of this calculation result is presented in the Fig. 4(a) which graphs the torque versus angle for various cases of Re. The overall profile of the torque curves are seen to deviate from the theoretical predictions of torque shown in Eq. (1) although computations and theory both predict the same extremal equilibria, 0° and 90°. The torques in the figure were normalized by dividing the maximum torque at $Re = 270$ and multiplied by 10, 200, and 4000 for $Re = 50, 5,$ and 0.1, respectively for better comparison and visualization. The curves in Fig. 4(a) for different Re shows torque free angles other than 0° and 90°, supporting the existence of metastability, especially at $Re = 0.1,$ and 5. These metastable angles appear in unstable and stable pairs and seem to be confined to the cases of low Re, possibly prior to the development of wake vortices which typically occur at $Re \approx 5 - 10$ (Zdravkovich, 1997). Despite the apparent deviation from theory, our numerics actually compares very well since the theoretical calculations are, after all, only valid in the regime where inertial effects dominate (Galdi & Vaidya, 2001). Fig. 4(a) also shows noticeable fluctuation of torque with angle, and also increasing magnitude with increasing effects of inertia, or Re. Because at the creeping flow regime,

any configuration is allowed, the trend observed from the simulation points to a monotonic, declining trend in equilibrium states with increasing *Re*, rather than a sharp change from infinitely many to two states, as was believed earlier.

Guided by experiments, we also investigate the impact of aspect ratio on the torque profile, although the experiments performed are for cylinders. Fig. 4(b) shows the normalized torque versus angle for $AR = 1.3, 2, 4$ and 8 where the torques are normalized by the maximum value of torque corresponding to $AR = 8$. The calculations are restricted to $AR > 1$, corresponding to prolate spheroids; the case of oblate spheroids ($AR < 1$) is similar. Results of our calculations indicate that ellipsoids with smaller *AR* (upto $AR = 2$) have higher propensity to display metastable states. Smaller *AR* display greater number of metastable states and also possess a higher degree of stability which is discussed in more detail in the following section. Previous studies (Chung et al., 2016) show that bodies with *AR* equal or close to 1 tend to autorotate even at small *Re* indicating that any orientation they assume is highly unstable. This could explain the behavior of the $AR = 1.3$ case. Therefore geometric effects also appear to play a significant role.

4. Discussion and conclusions

Our numerical computations and experiments point to the existence of metastable states in the context of orientation of hinged bodies in a flow whereas previous observations (in sedimentation and horizontal flow setups) have only reported the two extreme equilibrium orientations of 0° and 90°, also seen here. The stability of these new equilibria can be ascertained theoretically from the negativity of $\frac{d\mathcal{M}}{d\theta}$ at these equilibria. This observation points to new, interesting and heretofore unobserved physics in an otherwise well studied system. It is natural to ask if there are significant differences between terminal states observed in sedimentation versus horizontal flow experiments. The governing equations for linear and angular momentum on a rigid body sedimenting in a fluid reveal (Happel & Brenner, 1965) that the net torque has a contribution due to translational and rotational motion but only contains the latter in our study due to the absence of translation and gravitational effects. Furthermore, two of the torque components are constrained in the horizontal flow and fixed body setup. The differences between the two cases is by no means obvious and remains to be explored.

Since metastable states were not known previously, they may have been identified with the stable orientation. Earlier studies (Chung et al., 2016), performed for $0.5 < AR < 2.0$ indicate that bodies (cylinders) with higher *AR* maintain their stable state configurations up to much higher *Re* than those with lower *AR* (Chung et al., 2016, Fig. 5) supporting the importance of *AR* on the existence of metastability and pointing to the possible presence of these additional equilibria which contribute to longer residence in a dynamically stable state. The specific trends concerning the effect of *AR* observed in current and previous experiments are different from those noted here using our CFD approach in Section 3.2 but the range of *AR* in the two studies are different. This suggests a much more complex influence of geometry. Based on experiments, it appears that between $0.5 \leq AR \leq 2$, the body moves to the terminal steady state very rapidly but based on numerics, for $2 < AR \leq 8$, the number of metastable states decline. Geometric aspects of metastability need careful and extensive exploration in the future.

One significant and fundamental question raised by our experimental observations is regarding the nature of transitions and bifurcations in physical systems. We ask if transitions in physical systems are necessarily continuous? In order to understand the observed intermediate stable states, we need to look at the net torque imposed upon the body due to the flow. Following the argument used in Galdi (2002); Galdi and Vaidya (2001) we write the net torque ($\vec{\mathcal{M}}$) on a spheroid as

$$\vec{\mathcal{M}} = \vec{\mathcal{M}}_{in} + \vec{\mathcal{M}}_{oc} \tag{4}$$

where $\vec{\mathcal{M}}_{in}$ refers to the inertial contribution to torque and $\vec{\mathcal{M}}_{oc}$ is the torque due to off-centering of suspension (Galdi, 2002; Happel & Brenner, 1965). We can write these contributions in the specific vector form:

$$\vec{\mathcal{M}}_{in} = \left(\alpha_1 Re \sin 2\theta + \alpha_2(\theta) Re^2\right)\hat{e}_3 \tag{5}$$

$$\vec{\mathcal{M}}_{oc} = \vec{R} \times \vec{g} \tag{6}$$

where θ is the orientation angle, $\alpha_1 > 0$, α_2 are the torque coefficients, $\vec{R}$ is the vector from the center of gravity of the body to the point of suspension of the body and $\vec{g}$ is the acceleration due to gravity. Note that the Eq. (5) is a variation of the expression[4] obtained in Galdi (2002) for small *Re*. In the stable/metastable state we impose that $\vec{\mathcal{M}} = \vec{0}$ as a result of which θ is seen to depend on *Re*. Furthermore, if the off-centering effect is sufficiently small (as we believe to be in our experiments), $|\vec{\mathcal{M}}_{oc}| << 1$ and is negligible. Even when this effect is not neglected, it is independent of θ and *Re* and therefore just a constant and not the cause of the existence of the metastable states. While this argument is not rigorous, it strengthens our observational conclusions that the metastable transitions are indeed real and dynamically induced and reveals a plausible argument relating θ and *Re*.

[4] The first order, in *Re*, expression for $\vec{\mathcal{M}}_{in}$ proposed earlier (Galdi, 2002) is based on expanding velocity field $\vec{u} = \vec{u}_s + \vec{w}$, where the impact of flow field $\vec{w}$ on the torque is shown to be bounded above and sufficiently small. We assume that a similar expression for $\vec{u}$ can be used yielding a quadratic expression in *Re*.

The most commonly accepted cause for the dynamic settling of a spheroid/cylinder into its terminal stable state is the wake vortex. The onset of vortex shedding which results in a pressure and tangential stress differentials in the fore and aft regions of the body is thought to provide the necessary inertial torque to the body to turn it into its stable configuration. This argument appears to valid in the ideal, zero-friction, situation (see Fig. 4(c)). Numerical calculations reveal that metastability exists for the case of low *Re* and the torque profile curve shows that beyond $Re \approx 10$ torques vanish only at the two well known extremal angles indicating a connection between metastability and the onset of wake vortices. However, in the presence of friction, it is the magnitude of torque and its relative value compared to frictional resistance, which determines the transition behavior. The qualitative profile of θ vs. *Re*, however, remains the same in all cases. Therefore, in summary, metastability is a *real* phenomenon in this system, whether we are speaking in the 'real world' or 'ideal' sense. In this paper, we have focused merely on the issue of the *existence of metastability*. Several details regarding the details of the flow and body dynamics remain unknown. These issues will be discussed in our future publications on this subject.

Acknowledgments

We would like to thank Will Hernandez for his help with the experimental design. We would also like to thank Professor Giovanni Galdi for helpful discussions on this subject. Thanks to Professor Josh Galster for help with pressure measurements. The experimental was conducted with partial support from the SBIR grant at MSU. This material is based upon work supported by the National Science Foundation under Grant No. 1229113. The Authorship in the paper is alphabetical.

Appendix A. Statistical analysis

Table 2
Model for each individual and combined trials per direction and material type. Dev-expl = Deviance explained and p =p-value for the nonparametric function s(Re) in the additive model.

Material type	Individual trials		Combined trials		
	Adj-R^2 range	Dev expl range	Adj-R^2 range	Dev expl range	p
SW1	0.905–0.965	0.913–0.996	0.282	0.325	0.006
CW1.25	0.953–1.000	0.973–1.000	0.482	0.521	0.0003
S2	0.853–0.996	0.965–0.998	0.659	0.669	0
CR1.25	0.525–0.977	0.719–0.987	0.591	0.628	0
C0.75	0.823–0.930	0.863–0.945	0.02	0.033	0.967
C2.0	0.927–0.940	0.950–0.970	0.01	0.014	0.555
C1.0	0.854–0.945	0.898–0.968	0.411	0.471	0.01
S1	0.898–0967	0.917–0.978	0.038	0.071	0.357

Table 3
Model for all combined data. The angles for all 49 trials is fitted using an additive model (i.e. $\theta = f(\text{material type}) + g(\text{phase}) + s(Re)$) which incorporates the material type, phase and *Re* dependence. Each case of material type is compared with the reference case of CW1.25. For the dependence on *Re*, a fit with an $edf > 1$ and p-value zero, is indicative of a strong nonlinear relationship (Hastie & Tibshirani, 1990).

Covariates in the model		Coef estimate	p-value
Material type	SW1	−0.467	
	C2.0	18.212	
	C0.75	14.463	
	C1.0	2.342	0
	C1.25	−1.479	
	S1	8.635	
	S2	−17.724	
	CW1.25(ref)	0	
Re	s(Re)	$edf = 3.725$	0

References

Belmonte, A., Eisenberg, H., & Moses, E. (1998). *Physical Review Letters, 81*, 2.
Blevins, R. D. (1977). *Flow-induced vibration*. Van Nostrand Reinhold Co., New York.
Camassa, R., Chung, B., Howard, P., McLaughlin, R. M., & Vaidya, A. (2010). In A. Sequeira, & R. Rannacher (Eds.), *Advances in mathematical fluid mechanics* (pp. 135–145). Springer Verlag.
Chung, B. J., Cohrs, M., Ernst, W., Galdi, G., & Vaidya, A. (2016). *Archive of Applied Mechanics, 86*(4), 627–641.
Clift, R., Grace, J. R., & Weber, M. E. (2005). *Bubbles, drops, and particles*. Courier Corporation.
Falck, D., & Collette, B. (2012). *FreeCAD [How-to]. solid modeling with the power of python* p. 2012. Packt Publishing.
Fields, S. B., Klaus, M., Moore, M. G., & Nori, F. (1997). *Nature, 388*.
Galdi, G. P. (2002). In S. Friedlander (Ed.), *Handbook of mathematical fluid mechanics* (pp. 653–791). Elsevier Science, Amsterdam.
Galdi, G. P., & Vaidya, A. (2001). *Journal of Mathematical Fluid Mechanics, 3*.
Geuzaine, C., & Remacle, J. (2009). *International Journal for Numerical Methods in Engineering, 79*, 1309–1331.
Happel, V., & Brenner, H. (1965). *Low reynolds number hydrodynamics*. Prentice Hall.
Hastie, T. J., & Tibshirani, R. J. (1990). *Generalized additive models*. Chapman and Hall.
Horowitz, M., M., & Williamson, C. H. K. (2010). *Journal of Fluid Mechanics, 651*, 251–294.
Joseph, D. D., & Liu, Y. J. (1993). *Journal of Rheology, 37*.
Kirchoff, G. (1869). *Journal für die Reine und Angewandte Mathematik, 71*.
Lamb, H. (1895). *Hydrodynamics*. University Press.
Leal, L. G. (1980). *Annual Review of Fluid Mechanics, 12*.
Lugt, H. (1980). *Journal of Fluid Mechanics, 99*.
Lugt, H. (1983). *Annual Review of Fluid Mechanics, 15*.
Mahadevan, L., Ryu, W., & Samuel, A. D. T. (1999). *Physics of Fluids, 11*.
Mittal, R., & Iaccarino, G. (2005). Immersed boundary methods. *Annual Review of Fluid Mechanics, 37*, 239–261.
Pettyjohn, E. A., & Christiansen, E. B. (1948). *Chemical Engineering Progress, 44*.
Ruppert, D., Sheather, S. J., & Wand, M. P. (1995). *Journal of the American Statistical Association, 90*.
Sohankar, A., Norberg, C., & Davidson, L. (1998). *International Journal for Numerical Methods in Fluids, 26*, 39–56.
Tanabe, Y., & Kaneko, K. (1994). *Physical Review Letters, 73*(10).
Team, R. C. (2013). *R: A language and environment for statistical computing*. R Foundation for Statistical Computing, Vienna, Austria. URL http://www.R-project.org/.
Vaidya, A. (2006). *Journal of Fluids and Structures, 22*.
Williamson, C. H. K. (1996). *Annual Review of Fluid Mech., 28*.
Williamson, C. H. K., & Goverdhan, R. (2004). *Annual Review of Fluid Mechanics, 36*.
Willmarth, W. W., Hawk, N. E., Galloway, A. J., & Roos, F. W. (1967). *Journal of Fluid Mechanics, 27*(1).
Zdravkovich, M. M. (1997). *Flow around circular cylinders volume 1: fundamentals*. Oxford University Press.
Zdravkovich, M. M. (2002). *Flow around circular cylinders volume 2 applications*. Oxford University Press.